*Progress In Electromagnetics Research C, Vol. 133, 121–134, 2023*

# A Compact Dual-Band Octal Patch Loaded with Bow-Tie Parasitic MIMO Antenna Design for 5G mm-Wave Wireless Communication

**Idrish Shaik[1, *] and Krishna V. Sahukara[2]**

**Abstract**—In the present era of wireless communication networks, the key area of concern is always the need for faster data rates to meet the growing requirements. The 5G standards have the fortitude to bring about rapid data transfer speeds, instantaneous connectivity, large data capacities, and minimal latency. In this paper, a novel octal patch integrated with a bow-tie parasitic antenna element with full ground plane that incorporates a microstrip dual band antenna was proposed for 5G n257/n261/n259 and n260 band applications. This bow-tie parasitic antenna element integrated octal patch single and MIMO antenna structure was mounted on an RT Duriod 5880 ($\varepsilon_r$ = 2.2, loss tangent = 0.0009) with dimensions of $7.5 \times 9.9 \times 0.9\,\text{mm}^3$ and $7.5 \times 19.8 \times 0.9\,\text{mm}^3$ ($0.67\lambda \times 1.75\lambda \times 0.07\lambda$, where $\lambda$ is considered at the lowest operating tuned frequency). A decoupling element was precisely placed in the core of a two-element MIMO antenna to reduce the mutual coupling. This embedded antenna radiating structure resonated in dual bands ranging 26.69–29.55 GHz and 38.24–42.53 GHz with a center frequency of 28 GHz and 40.2 GHz, respectively. This achieves a bandwidth of 2.85 GHz (10.3%) and 4.29 GHz (10.75%) at the dual bands. The maximum gains were 7.9 dBi and 6.97 dBi, and greater than 92% efficiency was obtained over the dual bands. From the results extracted from the proposed antenna, it was found that the antenna is capable of covering the 5G NR n257/n261/n259 and n260 bands with significant bandwidth, gain, isolation, ECC, DG, TARC, multiplexing efficiency, CCL MEG, and radiation efficiency. Thus, the antenna can be considered a potential contender for 5G millimeter wave wireless communication systems.

## 1. INTRODUCTION

It was planned that the millimeter-wave frequency range would be utilized by the fifth-generation (5G) network, which would result in a significant improvement in the capacity of wireless technology [1]. In order to reach the significant capacity and throughput demands of future 5G networks, the spectrum now available at millimeter wave (mm-wave) frequencies is considered to be a likely choice [2]. The ever-increasing volume of data sent and the number of connected devices have had far-reaching consequences on people's personal and professional lives. It was foreseen that by 2020, the number of mobile networking devices would surpass 100 billion, thanks to the rapid rise of wireless cellular infrastructure and the ongoing expansion of the Internet of Things [3]. Because the number of user devices is growing at such a fast rate, there is a greater need for bandwidth in order to handle the ever-increasing volume of data [4]. The most distinctive characteristics of 5G technologies are the relatively fast transmission of data, the avoidance of any delay, and the wider availability of connectivity. For highly populated urban regions where connection demand is strong, the 5G millimeter waves offers a compromise of penetration, coverage, speed, and capacity [5]. The development of antennas for contemporary mobile devices is a difficult endeavor, according to all reports. The development of future global standards for 5G networks

*Received 3 March 2023, Accepted 22 May 2023, Scheduled 30 May 2023*
* Corresponding author: Idrish Shaik (idrishshaik@gmail.com).
[1] ECE Department, Andhra University, Vishakhapatnam, India. [2] ECE Department, GVP College for Degree and PG Courses (Autonomous), Vishakhapatnam, India.

needs antennas that are much more compact while retaining their capabilities. The design of an antenna is ascertained by the operating frequency as well as the needed bandwidth [6–8].

The implementation of sub-6 GHz and mm-wave frequencies presents additional hurdles for fifth generation wireless antennas. The design of antennas for the 5G mm-wave frequencies that have been designated can be somewhat demanding for antenna designers. The mm-wave spectrum experiences increasing levels of loss due to propagation and atmosphere [9]. Attenuation by the atmosphere will have a bigger effect on radio waves as their frequencies go up. The attenuation of signals in outer space is mostly due to atmospheric gas absorption. A $4 \times 4$ Multi-Input Multi-Output (MIMO) antenna array was presented in [10]. This antenna had a 25–40 GHz bandwidth and 16 dBi gain. Unfortunately, the design was enormous with $135 \times 97\,\text{mm}^2$. For high-gain dual-band applications, a small antenna for 28/38 GHz has been described. This antenna was developed in order to avoid the array's complexity as well as its enormous size [11]. A split-ring meta-surface was mounted over a patch covering the 28 GHz mm-wave spectrum in [12]. The antenna's highest gain was 11.94 dB, and its impedance bandwidth was 9.77 GHz after meta-surface use. The suggested antenna had a massive gain; however, it was MIMO incapable. The pros of the co-planar wave-guide slot antenna [13] for 28/38 GHz, including its simple construction, efficient broadband performance, and low dispersion, were recently published. It was also suggested that a small, simple-geometry, broadband antenna that could operate across 28 GHz, 38 GHz, or both, existed [14, 15]. Reports have shown that the devices in the industry should have a small stature, a wide frequency range, and a strong gain. Despite much investigation, there is still a dearth of high gain, as achieving such gains often requires either an array method or a significantly larger and more structurally sophisticated design.

As previously mentioned [16, 17], a MIMO antenna may provide better strength and a broader band, making it suitable for the needs of a 5G communication system. A high gain and broad antenna makes it possible to achieve a higher data rate and big user capacity [18]. The 8-element dual-band MIMO antenna proposed in [19] has a $150 \times 75\,\text{mm}^2$ dimension. Over 12 dB of separation was measured between elements. However, it only achieved a gain of 2.5 dBi and 5 dBi. MIMO systems depend on mutual coupling for high data rates. Parasitic elements, meta-materials, and defected ground structure (DGS) can diminish mutual coupling [20–22].

This proposed design offers small-scale single- and two-element MIMO antennas with dimensions of $7.5 \times 9.9 \times 0.9\,\text{mm}^3$ and $7.5 \times 19.8 \times 0.9\,\text{mm}^3$ respectively to be used for 5G mm-wave wireless applications. It resonates at 28 and 40 GHz and has bandwidths of 2.85 GHz and 4.25 GHz at dual bands, making it suitable for broadband. The antenna presented in this paper is composed of a patch with a parasitic element mounted on a Rogers 5880 substrate with a full ground plane at the bottom and also a decoupling element in the center of the two-element MIMO design to improve isolation and also offer dual bands of the required resonating frequency.

## 2. GEOMETRY OF ANTENNA DESIGN

Figure 1 illustrates the antenna only with one element that has been proposed from both the top and bottom views. The numerically calculated antenna dimensions are $7.5 \times 9.9 \times 0.9\,\text{mm}^3$. The presented monopole is designed with RT Duriod 5880 as a substrate, which has a dielectric constant of 2.2, a loss tangent of 0.0009, and a thickness of 0.9 mm. With CST Studio Suite 2019, the structure is designed, and simulation and evaluation of the structure are carried out. The octal patch has a complete ground plane at its bottom and an enhanced bow-tie parasitic element at its top. The excitation for the antenna is provided via a microstrip feed of 50 Ω. This combination enables the antenna to cover dual-bands, which range 26.69–29.55 GHz and 38.24–42.53 GHz.

### 2.1. Proposed Antenna Design Evolution Process

Figure 2 provides an illustration of each of the three stages that combine the evaluation process of the posited antenna. The patch and ground are designed using the dimensions specified in Table 1.

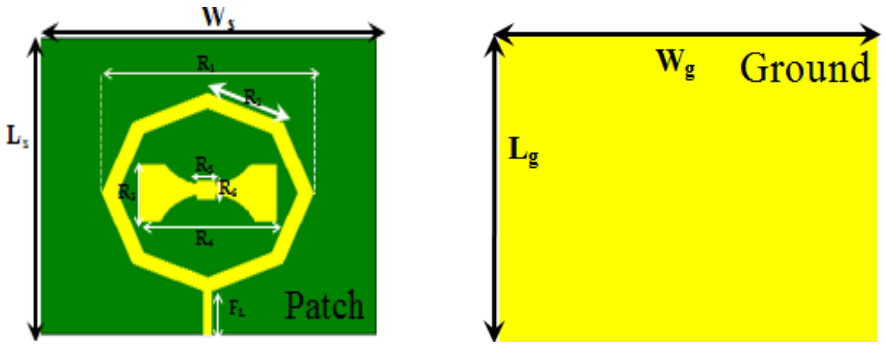


**Figure 1.** Posited antenna geometry of single element with full ground plane. (a) Top layer. (b) Bottom layer.

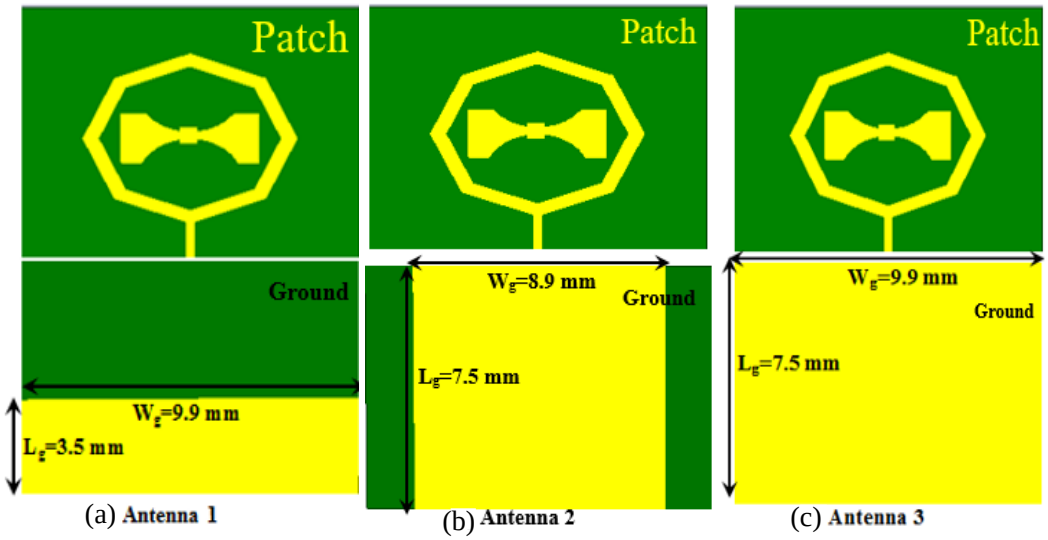


**Figure 2.** Antenna design evolution procedure. (a) Antenna-1. (b) Antenna-2. (c) Antenna-3.

**Table 1.** Calculated numerical design parameters of proposed antenna design in mm.

| **Parameter** | $L_S$ | $W_S$ | $L_g$ | $W_g$ | $R_1$ | $R_2$ | $R_3$ | $R_4$ |
|---|---|---|---|---|---|---|---|---|
| **Dimensions** | 7.5 | 9.9 | 7.5 | 9.9 | 6.3 | 2.4 | 1.4 | 4.1 |
| **Parameter** | $R_5$ | $R_6$ | $F_L$ | $R_7$ | $R_8$ | $R_9$ | $S$ | $h$ |
| **Dimensions** | 0.5 | 0.5 | 2.5 | 0.8 | 2.1 | 0.5 | 3.5 | 0.9 |

*2.1.1. Effect of Change in $L_g$ and $W_g$ of the Ground Plane*

This section's objective is to investigate the influence of the $L_g$ and $W_g$ parameters, one of the most significant considerations, while attempting to obtain a dual-band. The impact of increasing $L_g$ from 2 mm to 3.5 mm may be seen in the antenna-1 design shown in Figure 2(a) of the evaluation process and the return loss plot in Figure 3(a). A minor peak below −10 dB was obtained as a result of the length increase which can be seen in Figure 3(a). A single band was obtained. This particular single band had a broad bandwidth, and antenna-1 resonated at 26 GHz when the length was extended at 3.5 mm. Because of this change, the antenna-2 model was made with a vertical partial ground right at

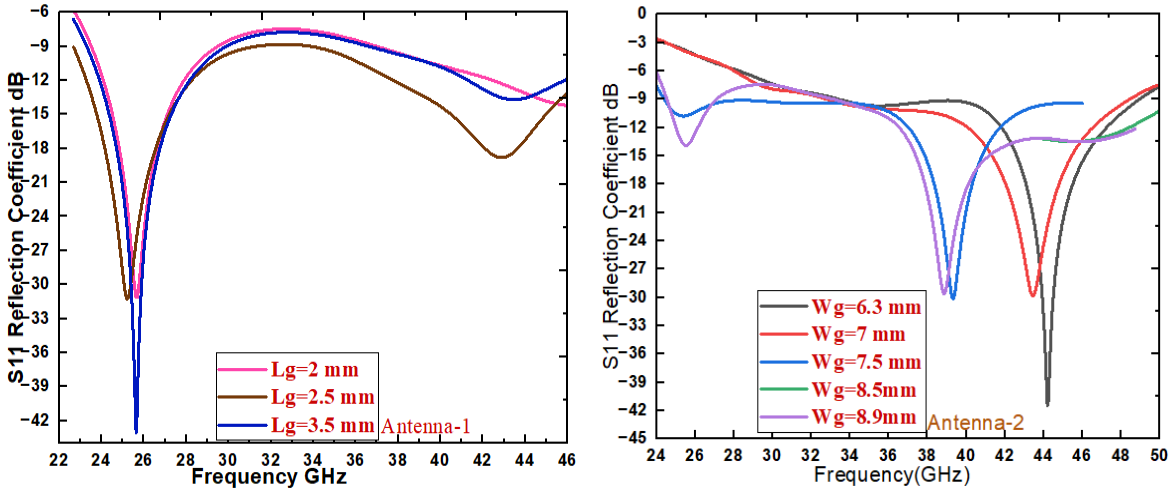


**Figure 3.** $S_{11}$ reflection coefficient. (a) Antenna-1. (b) Antenna-2.

the bottom of the patch. Nevertheless, changing the $W_g$ value from 6.3 mm to 8.9 mm results in a wider bandwidth than that when it was fixed at 6.3 mm, which is about 23 GHz, but the gain dropped from 7.43 dBi to 5.14 dBi. There is a shift in frequency that can be observed in Figure 3(b) as the width of the ground plane is changed from $W_g = 6.3$ mm to $W_g = 8.9$ mm. At $W_g = 8.9$ mm, there is also a minor peak that is less than $-10$ dB, noticed in magnitude at 26 GHz.

### *2.1.2. Proposed Single Element Antenna Design*

After the thorough discussion in Section 2.1.1 that was just accomplished by adjusting the $L_g$ and $W_g$ values, a few minor peaks are depicted in Figures 3(a) and 3(b). In order to achieve the dual bands, it is evident that the ground plane has to be expanded laterally, as seen in antenna-3 of Figure 2(c). Table 1 shows the dimensions of the patch, substrate, and ground that were used to make the antenna-3 model. Both the lower and higher resonances are found in positions that are a perfect match for the requirements 28/40 GHz. The computed reflection coefficient of the recommended dual-band antenna is shown in Figure 4(a). With a successful adaptation, dual bands are established at the resonating frequencies of 28 GHz ($-37$ dB return loss) and 40 GHz ($-20$ dB return loss) for $L_g = 7.5$ mm and $W_g = 9.9$ mm; thus, these values are considered to be the ideal values with respect to the suggested antenna. Figure 4(b) shows the gain obtained at dual bands around 7.4 dBi at 28 GHz and 6.9 dBi at 38 GHz for a single element. Figure 4(c) gives the efficiency obtained for single element around 98% and 95% at 28 and 38 GHz, respectively, with less complex structure than the models discussed in introduction, and Figure 4(d) shows the current distribution in the patch at the operating frequency of 28 GHz.

## 2.2. Dual-Band Two Element MIMO Antenna

After a single dual-band antenna has been developed, the two antenna components will be arranged using the spatial diversity method to produce the desired MIMO antenna, which works at 28 GHz and 40 GHz for mm-wave applications. Figure 5 illustrates the design for a two-element MIMO antenna that has dimensions of $7.5 \times 19.8 \times 0.9\,\text{mm}^3$ listed in Table 1. In this antenna, a parasitic element was placed precisely in the middle of two patch elements on the substrate in order to improve the isolation and prevent surface leakage current.

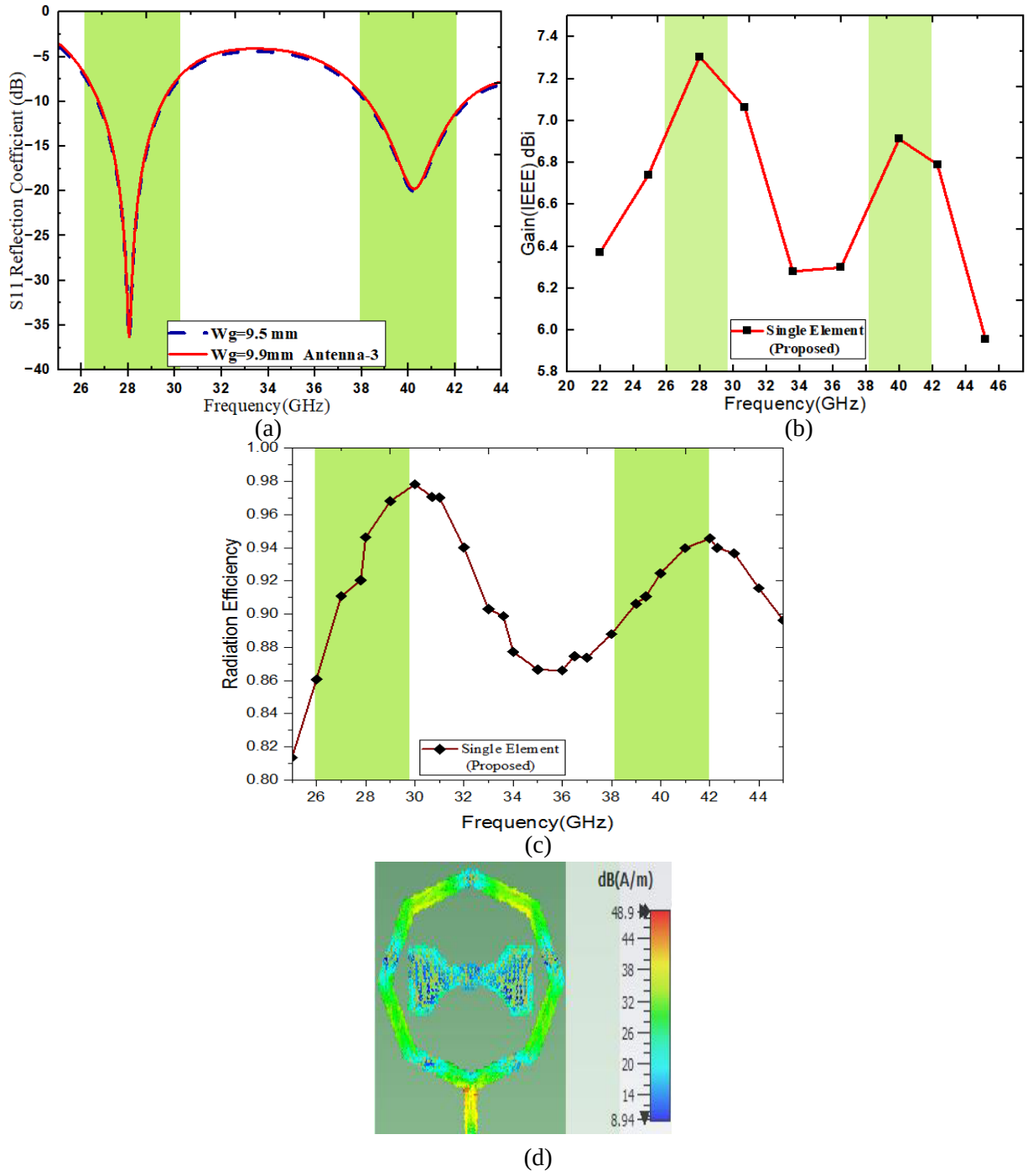


**Figure 4.** (a) $S_{11}$ reflection coefficient of proposed single element. (b) Gain (IEEE). (c) Single element radiation efficiency. (d) Single element current excitation in patch.

## 3. RESULTS WITH DISCUSSION

In this part, a detailed review of measured findings and simulated results is presented, along with an analysis of the proposed antenna performance based on a variety of different performance measures.

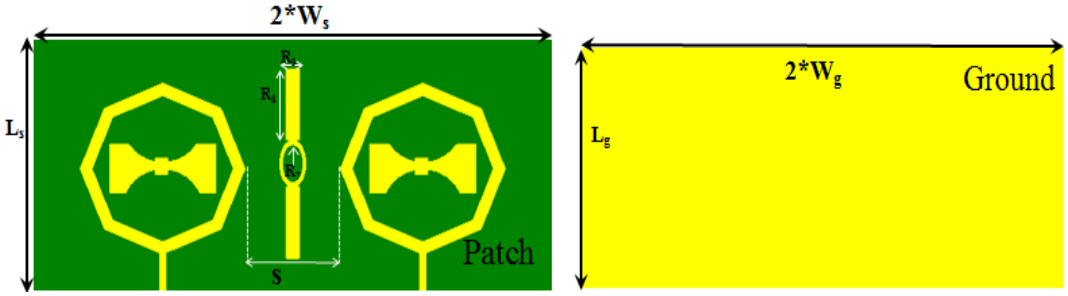


**Figure 5.** Posited antenna geometry of two-element MIMO antenna with full ground plane.

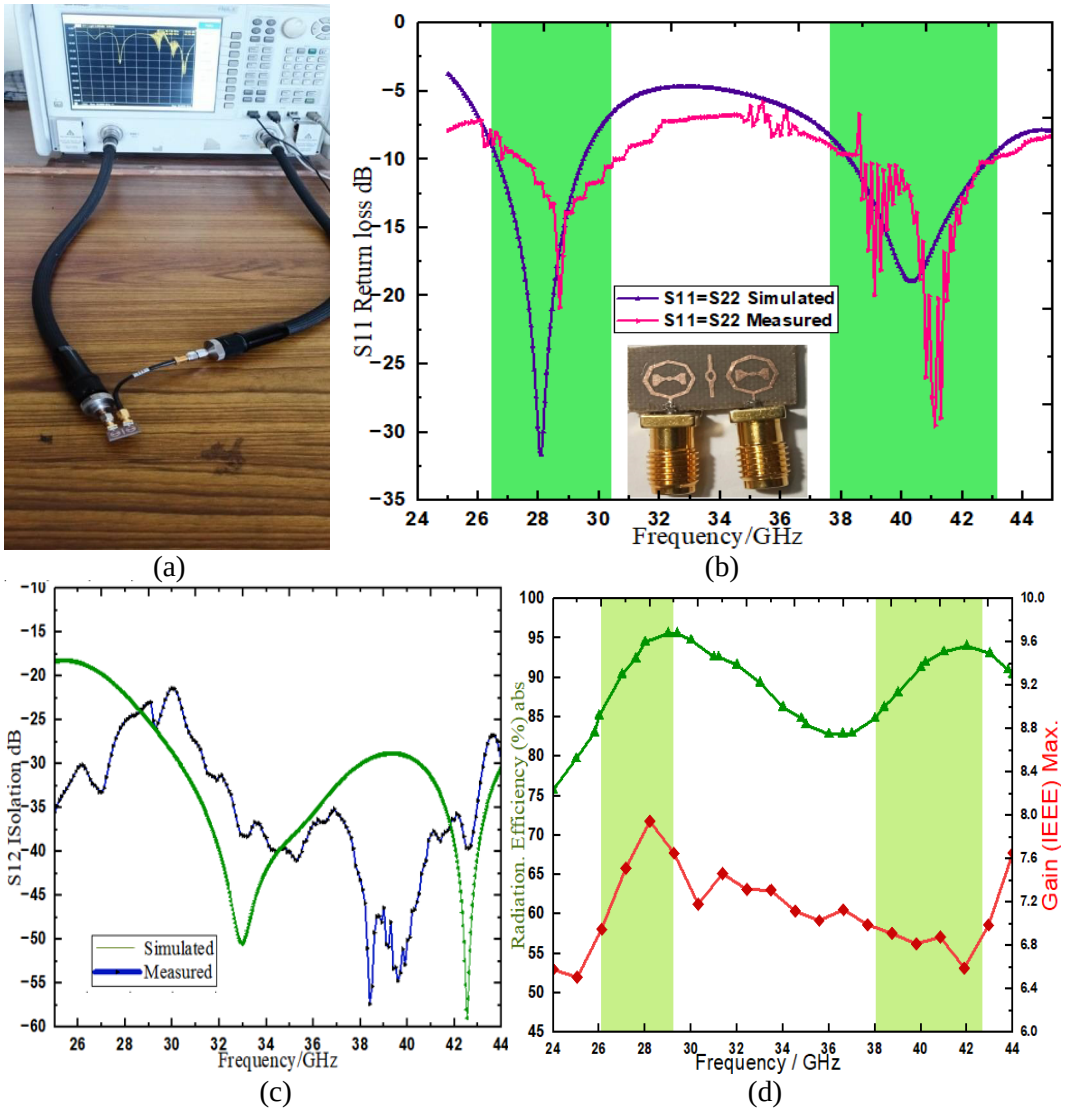


**Figure 6.** (a) Proposed antenna under test at VNA N5247A.09.90.02 with 2.42 mm convertible SMA connector probe. (b) Computed and experimented $S_{11}$ return loss of proposed antenna. (c) Computed and experimented $S_{12}$ of proposed antenna. (d) Peak gain and radiation efficiency.

### 3.1. Reflection Coefficient, Isolation, Peak Gain and Radiation Efficiency of MIMO Antenna

The designed antenna has an $S_{11}$ that is −37 dB and −18 dB at a resonating frequency of 28 GHz and 40 GHz, respectively. As a result of the symmetry of the recommended MIMO antenna ($S_{11} = S_{22}$, and $S_{12} = S_{21}$), only the $S_{11}$ as well as $S_{12}$ will be investigated. Figure 6(b) is an illustration of both the computed and measured return loss findings for the designed antenna. The proposed antenna design has bandwidths of 2.85 GHz and 4.29 GHz which allow it to cover frequency bands 28 GHz and 40 GHz. Figure 6(b) shows some distortion at the upper band's lower cutoff frequency. Nonetheless, the bandwidth has not been affected by this. The compact design, impacts of the SMA connection, and the measurement tolerances might all have an influence in the distortion. A picture of the fabricated antenna being tested using a 2.42 mm SMA connector attached to the Vector Network Analyzer (VNA) can be seen in Figure 6(a). The generated and measured values of the isolation parameters for $S_{12}$ are shown in Figure 6(c). An excellent impedance-matching characteristic is provided by the presented two-element MIMO radiator, together with isolation that is more than 20 dB at the dual bands. Figure 6(d) shows the gain plot and the minimum and maximum radiation efficiencies of the proposed antenna. The two-element MIMO structure provides gains of 7.9 dB and 6.9 dB as well as more than 92% efficiency obtained at dual bands of 28 GHz and 40 GHz, respectively. It was noticed that a significant gain enhancement compared to a single-element antenna was achieved. The results from both simulation and experiment have been proven in good agreement and are acceptable for the usage in applications requiring 5G connectivity.

### 3.2. Surface Current Distribution

The current excitation of the simulated antenna when one port is excited is shown and illustrated in Figures 7(a)–(d), which show the antenna in operation at its resonant frequency of 28 GHz and 40 GHz. The current distribution could be seen at the inset feed. As can be seen in Figures 7(a) and 7(c), in the absence of parasitic elements, the surface current of one element will flow into adjoining elements, which will result in a degradation of the MIMO antenna's radiation performance. Nonetheless, by including a

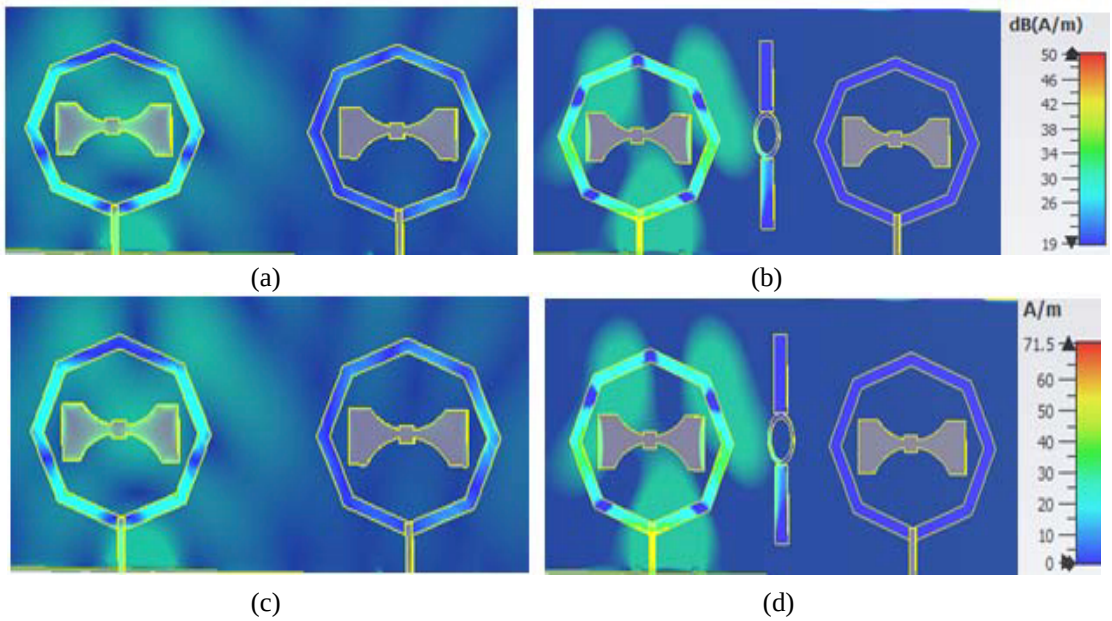


**Figure 7.** (a) Current excitation of posited antenna at 28 GHz without parasitic element. (b) Current excitation of posited antenna at 28 GHz with parasitic element. (c) Current excitation of posited antenna at 40 GHz without parasitic element. (d) Current excitation of posited antenna at 40 GHz with parasitic element.

parasitic element in the core of the proposed MIMO structure shown in Figures 7(b) and 7(d), surface currents may be suppressed, which helps in minimising the mutual coupling between two elements.

### 3.3. Characteristics of Electromagnetic Radiation

The three-dimensional polar plots of projected antenna structure are shown in Figures 8(a) and (b) for the resonant frequencies of 28 GHz and 40 GHz. Figures 8(c), (d), (e), and 8(f) show the radiation

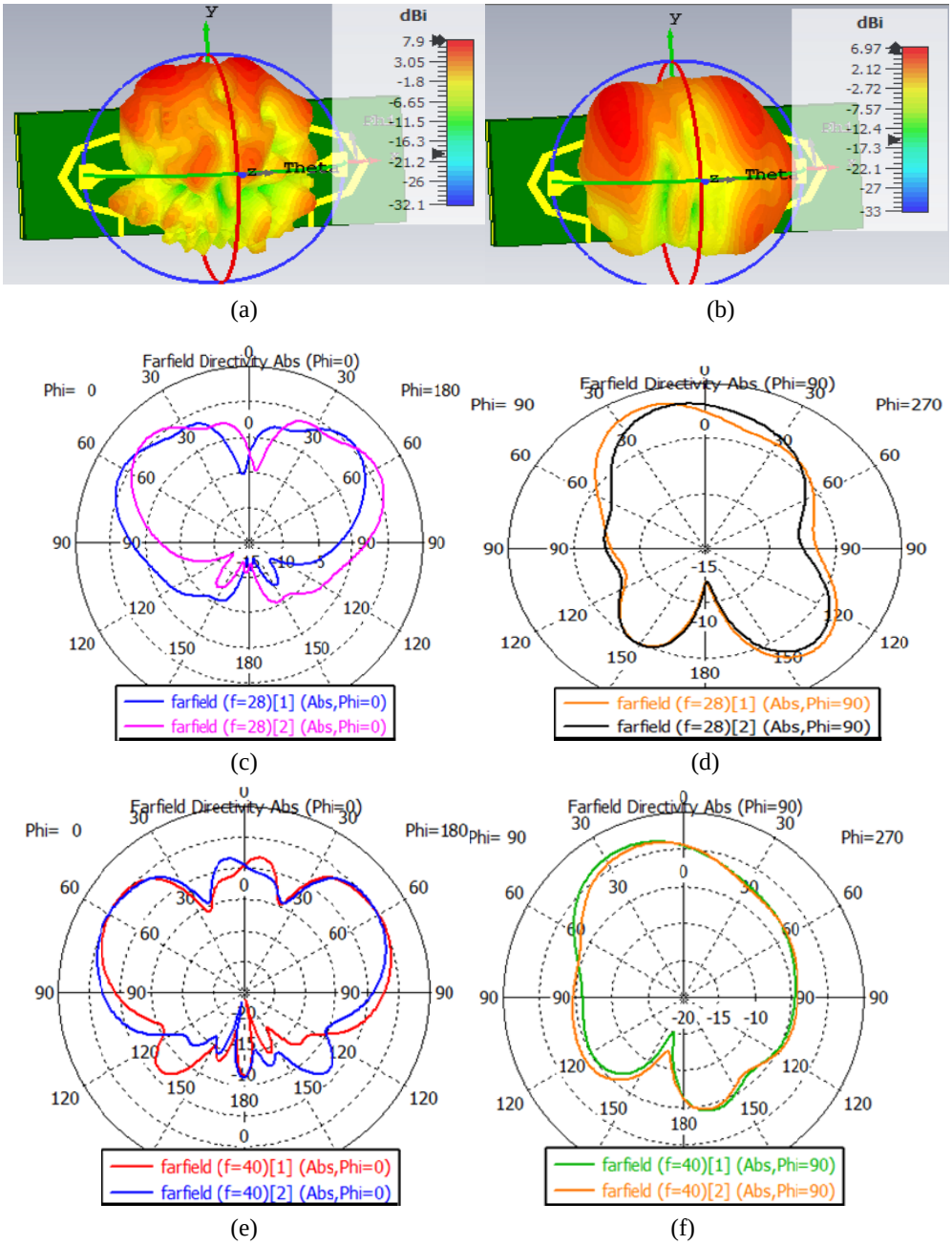


**Figure 8.** (a) 3D plot at 28 GHz, (b) 3D plot at 40 GHz, (c) polar plot at 28 GHz $E$-plane ($xoz$, $\emptyset = 0°$) and $H$-plane ($yoz$, $\emptyset =°$), (d) polar plot at 28 GHz $E$-plane ($xoz$, $\emptyset = 0°$) and $H$-plane ($yoz$, $\emptyset = 90°$), (e) polar plot at 40 GHz $E$-plane ($xoz$, $\emptyset = 0°$) and $H$-plane ($yoz$, $\emptyset = 0°$), (f) polar plot at 40 GHz $E$-plane ($xoz$, $\emptyset = 0°$) and $H$-plane ($yoz$, $\emptyset = 90°$).

pattern from the developed antenna design for the resonant frequencies of 28 GHz and 40 GHz, respectively. The polar plots in Figures 8(c) and 8(e) demonstrate that the major lobe orientation is ±60 degrees when phi equals 0° and 180°. At 28 GHz and 40 GHz, the 3 dB angular widths are 64° and 48°, respectively. Highly directional patterns may be seen in the computed polarization of the two major planes, $E$-plane ($XOZ$, $\emptyset = 0°$) and $H$-plane ($YOZ$, $\emptyset = 90°$) from Figures 8(c)–(f).

The suggested antenna is modelled using CST 2019 software, and a Rogers 5880 is used to fabricate a prototype of the antenna for the usage in practical applications. The top and bottom views of the fabricated element are shown in Figures 9(a) and 9(b).

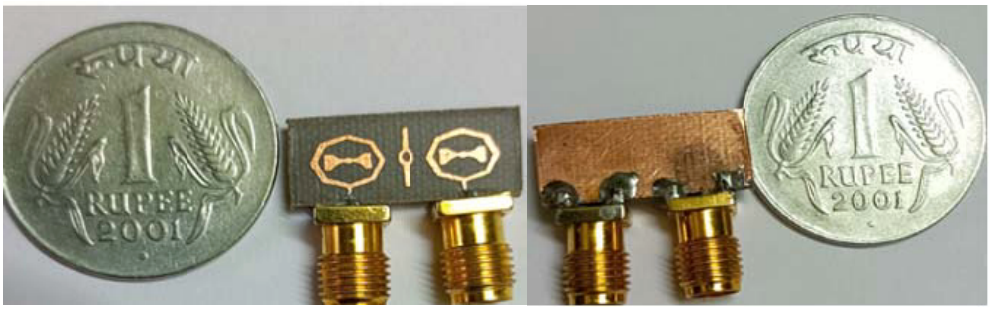


(a) (b)

**Figure 9.** (a) Top layer of the proposed antenna. (b) Bottom layer of the proposed fabricated antenna.

## 4. ANALYSIS OF THE TWO-ELEMENT MIMO ANTENNA PERFORMANCE OF THE SYSTEM

This section outlines measures to assess the proposed dual-band MIMO antenna. These characteristics include channel capacity loss (CCL), diversity gain (DG), radiation efficiency, gain, total active reflection coefficient (TARC), mean effective gain (MEG).

### 4.1. Envelope Correlation Coefficient, Diversity Gain (DG), and TARC

In MIMO systems, ECC is a key parameter that shows how each antenna element is independent based on its own properties [34]. The following expression in Equation (1) will be used in order to do a numerical calculation of ECC [35, 36]. The measured and simulated ECC values are calculated from $S$-parameters. The results in Figure 10(a) show that the ECC values over the dual bands are $< 0.002$

$$\rho_e \,(\text{or})\, \text{ECC}_{S\text{-parameters}} = \frac{\left|S_{11}^* S_{12} + S_{21}^* S_{22}\right|^2}{\left(1 - \left|S_{11}\right|^2 - \left|S_{21}\right|^2\right)\left(1 - \left|S_{22}\right|^2 - \left|S_{12}\right|^2\right)} \tag{1}$$

The diversity gain is a figure of merit used to measure the performance level of antenna diversity techniques [34]. The designed MIMO antenna diversity performance can be evaluated by using Equation (2) [35, 36]. The results in Figure 10(b) show that the DG is approx. 10 dB achieved over the dual bands.

$$\text{Diversity Gain (DG)} = \sqrt[10]{1 - \rho_e^2} \tag{2}$$

In the MIMO system the total active reflection coefficient is also necessary to evaluate exact behavior of MIMO system [36]. For a two-element MIMO system, the TARC can be calculated by using Equation (3) [35, 36].

$$\text{TARC}_{S\text{-parameters}} = \sqrt{\frac{(S_{11} + S_{12}e^{\varphi})^2 + (S_{21} + S_{22}e^{j\varphi})^2}{2}} \tag{3}$$

where $\varphi$ = phase difference, and the total active reflection coefficient (TARC) of the proposed structure is less than −20 dB in both operating bands which can be seen in Figure 10(c).

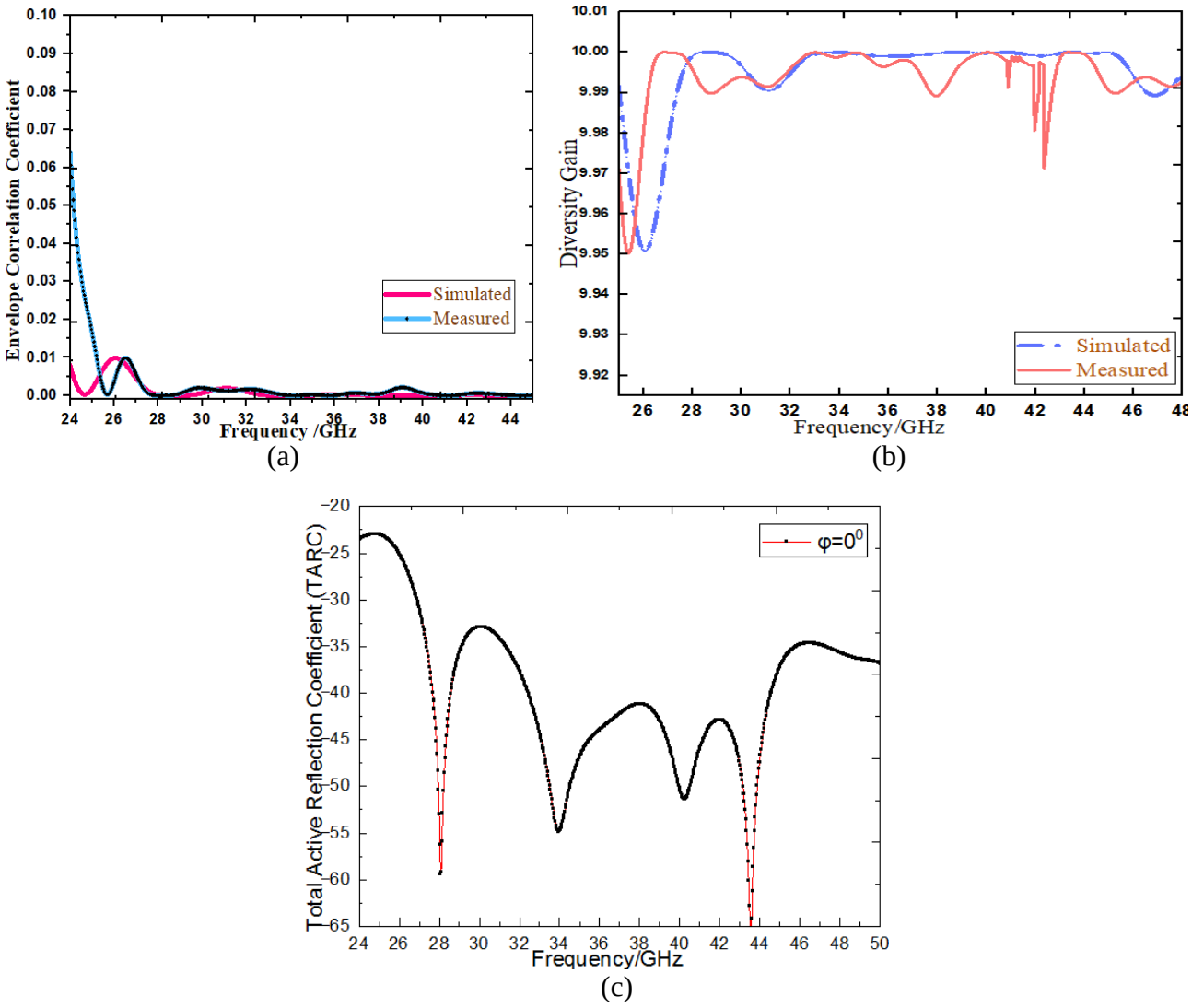


**Figure 10.** (a) Response of ECC. (b) Diversity gain response. (c) TARC response when $\varphi = 0°$.

### 4.2. Mean Effective Gain (MEG), Multiplexing Efficiency, and Channel Capacity Loss (CCL)

The antenna's potential to receive electromagnetic signals in a multipath environment is described by a quantity called the mean effective gain (MEG), which acts as an indication of diversity performance. The MEG of the designed antenna can be determined with Equation (4) [35, 36]. The measured and simulated MEG plots are shown in Figure 11(a). It has been determined that the antenna produces MEG of $< 3$ dB among both bands simultaneously.

$$\text{MEG} = 0.5 \left[ 1 - \sum_{j=0}^{n} |S_{ij}|^2 \right] \tag{4}$$

where '$n$' is the number of elements, and $i$ & '$j$' are the elements individually.

For a more realistic assessment of MIMO antenna performance, the multiplexing efficiency must be taken into consideration. It is attainable to calculate the multiplexing efficiency for a two-element

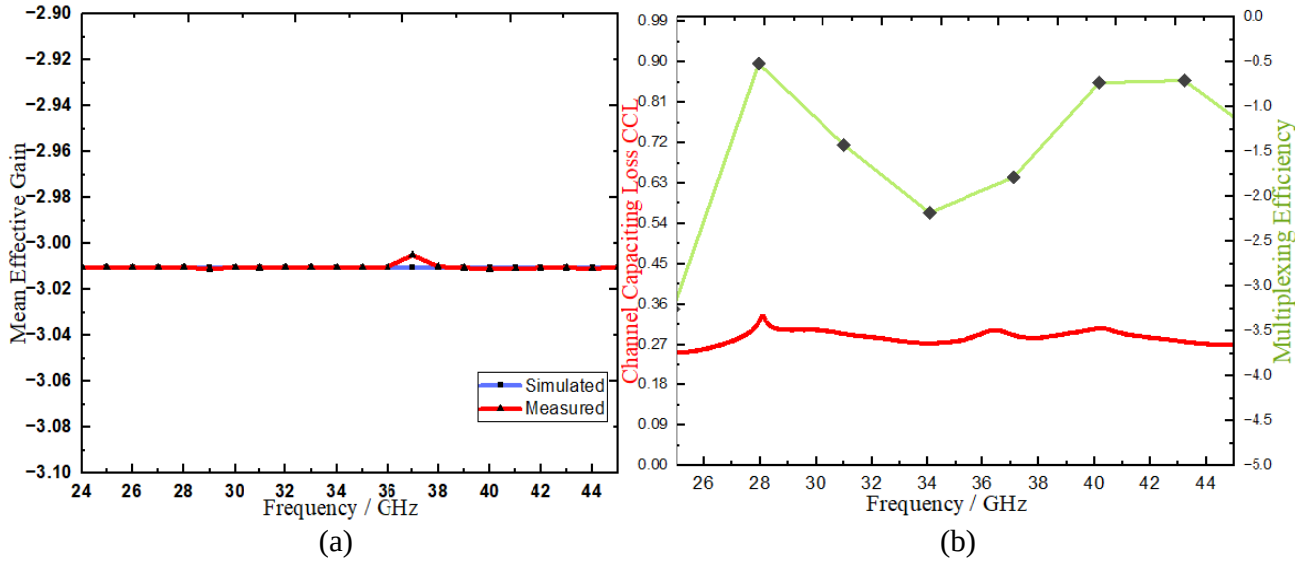


**Figure 11.** (a) Response of mean effective gain, (b) characteristics of multiplexing efficiency and CCL.

MIMO system using Equation (5) [34–36].

$$\text{Multiplexing efficiency}\,(\eta_{mux}) = \sqrt{(1 - \text{ECC}^2 \prod_{i=1}^{n} \eta_i} \tag{5}$$

where $\eta_i$ is the overall efficiency of individual element of MIMO radiator, and more than $-3$ dB of multiplexing efficiency was obtained, as seen in Figure 11(b).

The channel loss defines amount of data lost due to interference between channels is measured by the CCL using Equations (6)–(9). When antenna components are not properly separated, they might cause significant capacity loss due to mutual coupling.

$$\text{channel capacity loss}\,(\text{ccl}) = -\log_2 \det(\gamma_r) \tag{6}$$

$$\gamma_r = \begin{pmatrix} \rho_{11} & \rho_{12} \\ \rho_{21} & \rho_{22} \end{pmatrix} \tag{7}$$

where

$$\rho_{11} = 1 - \left(|S_{11}|^2 + |S_{12}|^2\right); \quad \rho_{12} = (s_{11}^* s_{12} + s_{21}^* s_{22}) \tag{8}$$

$$\rho_{22} = 1 - \left(|S_{21}|^2 + |S_{22}|^2\right); \quad \rho_{21} = (s_{22}^* s_{21} + s_{12}^* s_{21}) \tag{9}$$

In order to get the intended effect, the CCL must have a level that is lower than 0.4 bps/Hz. The CCL for the proposed antenna is lower than 0.3 bps/Hz over the dual-bands, as shown by Figure 11(b).

### 4.3. Comparative Analysis

Table 2 analyzes designed antenna to studies that have already been published in the past. The proposed antenna possesses beneficial radiation characteristics, including a wide bandwidth, steady gain, and high radiation efficiency. These characteristics give support to the concept that the design is acceptable with connection to systems of communication that operate within the band.

**Table 2.** Comparison of the designed antenna results with previous works.

| Ref. | Scale ($mm^2$) | Tuned Frequency (GHz) | No of Elements | BW (GHz) | Gain (dBi) | Rad. Eff. % | Mutual Coupling (dB) $< -15$ dB | ECC $< 0.5$ | DG $< 10$ |
|---|---|---|---|---|---|---|---|---|---|
| p* | $7.5 \times 19.8$ | 28/40 | 2 | 2.82, 4.29 | 7.9/6.97 | $> 92$ | $< -20$ | $< 0.001$ | $< 10$ |
| [23] | $7.5 \times 8.8$ | 28/38 | 2 | 1.23, 1.06 | 6.6/5.86 | $> 80$ | $< -24$ | $< 0.005$ | $< 10$ |
| [24] | $14 \times 12$ | 28/38 | 2 | 2.6, 2 | 1.27/1.83 | $> 76$ | $< -20$ | $< 0.004$ | $< 10$ |
| [25] | $26 \times 11$ | 27/39 | 2 | 2.9/4 | 5/5.7 | $> 98$ | $< -18$ | $< 0.001$ | $< 10$ |
| [26] | $12 \times 25.4$ | 28/33/37 | 2 | 11.7 | 6.4/7.2/5 | - | $< -20$ | $< 0.005$ | $< 10$ |
| [27] | $55 \times 110$ | 28/38 | 2 | 1.06/1.43 | 7.8/9.49 | $> 88$ | $< -27$ | $< 0.001$ | - |
| [28] | $6 \times 6$ | 28/34/45 | 4 | 1.2/0.92/1 | 13.5/11.2/13.7 | $> 90$ | - | - | - |
| [29] | $30 \times 35$ | 27.5–28.5 | $4 \times 2$ | 1 | 12 | $> 90$ | $< -40$ | $< 0.003$ | $< 9.9$ |
| [30] | $12.8 \times 26$ | 32.3–54.6 | 2 | 22 | 7.12 | $> 82$ | $< -33$ | $< 0.001$ | - |
| [31] | $28 \times 28$ | 28/38 | 4 | 4/5 | 9.5/11.5 | $> 80$ | $< -40$ | $< 0.003$ | $< 10$ |
| [32] | $14 \times 20$ | 17–25 | 2 | 8 | 8.4 | $> 80$ | $< -30$ | $< 0.01$ | - |
| [33] | $30 \times 15$ | 28 | 2 | 6 | 5.4 | $> 84$ | $< -35$ | $< 0.03$ | $< 10$ |

* proposed, - Not mentioned

## 5. CONCLUSION

A small-scale, high-performance single and two-element MIMO antennas have been thoroughly presented to report a dual-band frequency of 28/40 GHz. The design includes an octal patch integrated with a bow-tie parasitic element and a parasitic element in the center of the two-element MIMO design to improve isolation and also offer dual bands of the required resonating frequency. The design was implemented on a Rogers's 5880 substrate, which has a frequency center of 28/40 GHz, and it works significantly better than the antennas that are described in the previous works. Based on the results of both measured and simulated data, a significant improvement in the isolation obtained by adding a parasitic element in the center of the patches is obtained by the proposed antenna, which also has bandwidths of 2.85 GHz and 4.29 GHz at dual bands with peak gains of 7.9 dBi and 6.97 dBi over the operating bands. The analysis of the proposed antenna in the previous work shows that the designed antenna is feasible for 5G mm-wave wireless applications like ultra-high definition multimedia, which require high data rates and bandwidth, especially in cellular infrastructure.

## ACKNOWLEDGMENT

The authors would like to use this opportunity to acknowledge their gratitude to the administrations of both Bapatla Engineering College and GVPCDPGC for their support with this endeavor.

## REFERENCES

1. Andrews, J. G., S. Buzzi, W. Choi, et al., "What will 5G be?" *IEEE Journal on Selected Areas in Communications*, Vol. 32, No. 6, 1065–1082, 2014, doi: 10.1109/JSAC.2014.2328098.
2. Rappaport, T. S., S. Sun, R. Mayzus, et al., "Millimeter wave mobile communications for 5G cellular: It will work!," *IEEE Access*, Vol. 1, 335–349, 2013, doi: 10.1109/ACCESS.2013.2260813.

3. Attaran, M., "The impact of 5G on the evolution of intelligent automation and industry digitization," *J. Ambient Intel. Human Computer*, 2021, doi: 10.1007/s12652-020-02521-x.
4. Cao, Y., K. S. Chin, W. Che, W. Yang, and E. S. Li, "A compact 38 GHz multibeam antenna array with multifolded butler matrix for 5G applications," *IEEE Antennas and Wireless Propagation Letters*, Vol. 16, 2996–2999, 2017, doi: 10.1109/LAWP.2017.2757045.
5. Al-Gburi, A. J. A., Z. Zakaria, H. Alsariera, M. F. Akbar, I. M. Ibrahim, K. S. Ahmad, S. Ahmad, and S. S. Al-Bawri, "Broadband circular polarised printed antennas for indoor wireless communication systems: A comprehensive review," *Micromachines*, 2022, doi: 10.3390/mi13071048.
6. Ikram, M., E. A. Abbas, N. Nguyen-Trong, K. H. Sayidmarie, and A. Abbosh, "Integrated frequency-reconfigurable slot antenna and connected slot antenna array for 4G and 5G mobile handsets," *IEEE Transactions on Antennas and Propagation*, Vol. 67, No. 12, 7225–7233, Dec. 2019, doi: 10.1109/TAP.2019.2930119.
7. Shafi, M., A. F. Molisch, P. J. Smith, et al., "5G: A tutorial overview of standards, trials, challenges, deployment, and practice," *IEEE Journal on Selected Areas in Communications*, Vol. 35, No. 6, 1201–1221, Jun. 2017, doi: 10.1109/JSAC.2017.2692307.
8. Balanis, C. A., *Antenna Theory: Analysis and Design*, John Wiley and Sons, 1997.
9. Shayea, I., T. A. Rahman, M. H. Azmi, and M. R. Islam, "Real measurement study for rain rate and rain attenuation conducted over 26 GHz microwave 5G link system in Malaysia," *IEEE Access*, Vol. 6, 19044–19064, 2018, doi: 10.1109/access.2018.2810855.
10. Sethi, W. T., M. A. Ashraf, A. Ragheb, A. Alasaad, and S. A. Alshebeili, "Demonstration of millimeter wave 5G setup employing high-gain Vivaldi array," *International Journal of Antennas and Propagation*, 1–12, 2018, doi: 10.1155/2018/3927153.
11. Jilani, S. F. and A. Alomainy, "A multiband millimeter-wave 2-D array based on enhanced Franklin antenna for 5G wireless systems," *IEEE Antennas and Wireless Propagation Letters*, Vol. 16, 2983–2986, 2017, doi: 10.1109/lawp.2017.2756560.
12. Jeong, M. J., N. Hussain, J. W. Park, S. G. Park, S. Y. Rhee, and N. Kim, "Millimeter-wave microstrip patch antenna using vertically coupled split ring metaplate for gain enhancement," *Microwave and Optical Technology Letters*, Vol. 61, No. 10, 2360–2365, 2019, doi: 10.1002/mop.31908.
13. Ali, M. M. M. and A.-R. Sebak, "Dual band (28/38 GHz) CPW slot directive antenna for future 5G cellular applications," *2016 IEEE International Symposium on Antennas and Propagation (APSURSI)*, 2016, doi: 10.1109/aps.2016.7695908.
14. Przesmycki, R., M. Bugaj, and L. Nowosielski, "Broadband microstrip antenna for 5G wireless systems operating at 28 GHz," *Electronics*, Vol. 10, No. 1, 1, 2020, doi: 10.3390/electronics10010001.
15. Hussain, M., S. M. R. Jarchavi, S. I. Naqvi, U. Gulzar, S. Khan, M. Alibakhshikenari, and I. Huynen, "Design and fabrication of a printed tri-band antenna for 5G applications operating across Ka-, and V-band spectrums," *Electronics*, Vol. 10, No. 21, 2674, 2021, doi: 10.3390/electronics10212674.
16. Marzouk, H. M., M. I. Ahmed, and A. H. A. Shaalan, "Novel dual-band 28/38 GHz MIMO antennas for 5G mobile applications," *Progress In Electromagnetics Research C*, Vol. 93, 103–117, 2019.
17. Farahat, A. E. and K. F. A. Hussein, "28/38 GHz dual-band Yagi-Uda antenna with corrugated radiator and enhanced reflectors for 5G MIMO antenna systems," *Progress In Electromagnetics Research C*, Vol. 101, 159–172, 2020.
18. El Hadri, D., A. Zakriti, A. Zugari, M. El Ouahabi, and J. El Aoufi, "High isolation and ideal correlation using spatial diversity in a compact MIMO antenna for fifth-generation applications," *International Journal of Antennas and Propagation*, 1–10, 2020, doi: 10.1155/2020/2740920.
19. Zahid, M. N., Z. Gaofeng, S. H. Kiani, et al., "H-shaped eight-element dual-band MIMO antenna for sub-6 GHz 5G smartphone applications," *IEEE Access*, Vol. 10, 85619–85629, 2022, doi: 10.1109/ACCESS.2022.3189658.

20. Yon, H., N. H. A. Rahman, M. A. Aris, M. H. Jamaluddin, I. K. C. Lin, H. Jumaat, F. N. M. Redzwan, and Y. Yamada, "Development of C-shaped parasitic MIMO antennas for mutual coupling reduction," *Electronics*, Vol. 10, No. 19, 2431, 2021, doi: 10.3390/electronics10192431.
21. Alanazi, M. D. and S. K. Khamas, "A compact dual band MIMO dielectric resonator antenna with improved performance for mm-Wave applications," *Sensors*, Vol. 22, No. 13, 5056, 2022, doi: 10.3390/s22135056.
22. Awan, W. A., M. Soruri, M. Alibakhshikenari, and E. Limiti, "On-demand frequency switchable antenna array operating at 24.8 and 28 GHz for 5G high-gain sensors applications," *Progress In Electromagnetics Research M*, Vol. 108, 163–173, 2022.
23. Farahat, A. E. and K. F. A. Hussein, "Dual-band (28/38 GHz) wideband MIMO antenna for 5G mobile applications," *IEEE Access*, Vol. 10, 32213–32223, 2022, doi: 10.1109/ACCESS.2022.3160724.
24. Hasan, M. N., S. Bashir, and S. Chu, "Dual band omnidirectional millimeter wave antenna for 5G communications," *Journal of Electromagnetic Waves and Applications*, Vol. 33, No. 12, 1581–1590, 2019, doi: 10.1080/09205071.2019.1617790.
25. Ali, W., S. Das, H. Medkour, and S. Lakrit, "Planar dual-band 27/39 GHz millimeter-wave MIMO antenna for 5G applications," *Microsyst. Technol.*, Vol. 27, No. 1, 283–292, 2021, doi: 10.1007/s00542-020-04951-1.
26. Venkateswara Rao, M., B. T. P. Madhav, J. Krishna, Y. Usha Devi, T. Anilkumar, and B. Prudhvi Nadh, "CSRR-loaded T-shaped MIMO antenna for 5G cellular networks and vehicular communications," *International Journal of RF and Microwave Computer-Aided Engineering*, e21799, 2019, doi: 10.1002/mmce.21799.
27. Marzouk, H. M., M. I. Ahmed, and A. H. A. Shaalan, "Novel dual-band 28/38 GHz MIMO antennas for 5G mobile applications," *Progress In Electromagnetics Research C*, Vol. 93, 103–117, 2019.
28. Khattak, M. I., A. Sohail, U. Khan, Z. Barki, and G. Witjaksono, "Elliptical slot circular patch antenna array with dual band behavior for future 5G mobile communication networks," *Progress In Electromagnetics Research C*, Vol. 89, 133–147, 2019.
29. Bilal, M., S. I. Naqvi, N. Hussain, Y. Amin, and N. Kim, "High-isolation MIMO antenna for 5G millimeter-wave communication systems," *Electronics*, Vol. 11, No. 6, 962, 2022, doi: 10.3390/electronics11060962.
30. El Hadri, D., A. Zugari, and A. Zakriti, "Extra wide band MIMO antenna with high isolation and low correlation at 38 GHz mm-Wave frequency band for 5G applications," *E3S Web Conference*, 351 01076, 2022, doi: 10.1051/e3sconf/202235101076.
31. Hussain, M., W. A. Awan, E. M. Ali, M. S. Alzaidi, M. Alsharef, D. H. Elkamchouchi, A. Alzahrani, and M. F. Abo Sree, "Isolation improvement of parasitic element-loaded dual-band MIMO antenna for mm-Wave applications," *Micromachines*, Vol. 13, 1918, 2022, doi: 10.3390/mi13111918.
32. Sehrai, D. A., M. Asif, J. Khan, M. Abdullah, W. A. Shah, S. Alotaibi, and N. Ullah, "A high-gain and wideband MIMO antenna for 5G mm-Wave-based IoT communication networks," *Appl. Sci.*, Vol. 12, 9530, 2022, doi: 10.3390/app12199530.
33. Hussain, N., W. A. Awan, W. Ali, S. I. Naqvi, A. Zaidi, and T. T. Le, "Compact wideband patch antenna and its MIMO configuration for 28 GHz applications," *AEU — International Journal of Electronics and Communications*, Vol. 132, 153612, 2021, doi: 10.1016/j.aeue.2021.153612.
34. Khalid, M., S. I. Naqvi, N. Hussain, M. U. Rahman, and Y. Amin, "4-port MIMO antenna with defected ground structure for 5G millimeter wave applications," *Electronics*, Vol. 9, No. 1, 71, 2020, doi: 10.3390/electronics9010071.
35. Blanch, S., J. Romeu, and I. Corbella, "Exact representation of antenna system diversity performance from input parameter description," *Electronics Letters*, Vol. 39, No. 7, 705, 2003, doi: 10.1049/el:20030495.
36. Sharawi, M., *Printed MIMO Antenna Engineering*, Artech House, Norwood, MA, USA, 2014, ISBN 9781608076819.